 CMES, vol.57, no.2, pp.109-135, 2010

Solving Elastic Problems with Local Boundary Integral Equations (LBIE) and Radial Basis Functions (RBF) Cells

E. J. Sellountos[1], A. Sequeira[1] and D. Polyzos[2]

Abstract: A new Local Boundary Integral Equation (LBIE) method is proposed for the solution of plane elastostatic problems. Non-uniformly distributed points taken from a Finite Element Method (FEM) mesh cover the analyzed domain and form background cells with more than four points each. The FEM mesh determines the position of the points without imposing any connectivity requirement. The key-point of the proposed methodology is that the support domain of each point is divided into parts according to the background cells. An efficient Radial Basis Functions (RBF) interpolation scheme is exploited for the representation of displacements in each cell. Tractions in the interior domain are avoided with the aid of the companion solution. At the intersections between the local domains and the global boundary, tractions are treated as independent variables with the use of conventional boundary elements. Criteria about the size of the support domains are provided. The integration in support domains is performed easily, fast and with high accuracy. Due to the geometric information provided by the cells the extension of the method to three dimensions is straightforward. Three representative numerical examples demonstrate the achieved accuracy of the proposed LBIE methodology.

Keywords: Local Boundary Integral Equation (LBIE), meshless methods, elastostatic analysis

1 Introduction

After the pioneering work of [Zhu, Zhang, and Atluri (1998)], the Local Boundary Integral Equation (LBIE) method has been established as an excellent alternative to the Boundary Element Method (BEM), since it circumvents problems associated with mesh, fully populated matrices and lack of fundamental solutions. As

[1] Department of Mathematics and CEMAT, Instituto Superior Técnico, Technical University of Lisbon, Lisbon, Portugal.

[2] Department of Mechanical Engineering and Aeronautics, University of Patras, Greece Institute of Chemical Engineering and High Temperature Process ICETH-FORTH, Rio, Greece.

it appears in [Zhu, Zhang, and Atluri (1998)], the LBIE method is characterized as "truly meshless" since no background cells are required for the numerical evaluation of the involved integrals. Properly distributed nodal points, without any connectivity requirement, covering the domain of interest as well as the surrounding global boundary are employed instead of any boundary or finite element discretization. All nodal points belong to regular sub-domains (e.g. circles for two-dimensional problems) centered at the corresponding collocation points. The fields at the local and global boundaries as well as in the interior of the sub-domains are usually approximated by the Moving Least Squares (MLS) approximation scheme. The local nature of the sub-domains leads to a sparse linear system of equations and after proper renumbering to a banded system.

In the framework of linear elasticity, the first LBIE methodology is due to [Atluri, Sladek, Sladek, and Zhu (2000)]. Their work can be considered as a direct extension to elastostatics of the work of [Zhu, Zhang, and Atluri (1998)], on potential problems. After the aforementioned work, several papers dealing with LBIE solutions of linear elastic problems appeared in the literature, such as those of [Sladek, Sladek, Atluri, and Keer (2000)], [Sladek, Sladek, and Keer (2003)], [Sladek, Sladek, and Atluri (2002)], [Atluri, Han, and Shen (2003)], [Han and Atluri (2003)], [Sellountos and Polyzos (2003)], [Sellountos and Polyzos (2005b)], [Sellountos and Polyzos (2005a)], [Sellountos, Vavourakis, and Polyzos (2005)], [Bodin, Ma, Xin, and Krishnaswami (2006)], [Vavourakis, Sellountos, and Polyzos (2006)] [Zhu, Zhang, and Wang (2007)], [Vavourakis and Polyzos (2007)], [Vavourakis and Polyzos (2008)], [Vavourakis (2008)], [Vavourakis (2009)] [Vavourakis, Protopappas, Fotiadis, and Polyzos (2009)], [Sladek, Sladek, Solek, Tan, and Zhang (2009)] and [Sellountos, Sequeira, and Polyzos (2009)]. A comprehensive presentation of meshless LBIE methods can be found in the books of [Atluri and Shen (2002)] and [Atluri (2004)].

After the work of [Atluri, Sladek, Sladek, and Zhu (2000)], [Sellountos and Polyzos (2003)] used the LBIE method for solving frequency domain elastic problems. The new features of the latter work were i) the treatment of boundary displacements and tractions as independent variables thereby avoiding the MLS derivatives, and ii) the use of a relatively uniform distribution of points so that in the global boundary the MLS interpolation to possess the δ - property [Gosz and Liu (1996)] which permits the imposition of the essential boundary conditions directly to the fictitious values. However, although accurate, the requirement for relatively uniform distribution of points confines the use of the method to structures with regular shapes.

In order to avoid the requirement of using uniformly distributed points, [Vavourakis and Polyzos (2007)] and [Vavourakis and Polyzos (2008)] proposed an LBIE/MLS method where both singular and hypersingular LBIEs are used for the represen-

tation of displacement and traction fields. The problem in this approach is the treatment of displacements and stresses as independent variables everywhere in the analyzed domain, a fact that increases drastically the degrees of freedom, rendering the method prohibitive for large structures.

Very recently, [Sellountos, Sequeira, and Polyzos (2009)] combined the LBIE method of [Sellountos and Polyzos (2003)] with the Radial Basis Functions (RBF) scheme [Sellountos and Sequeira (2008a)], [Sellountos and Sequeira (2008b)] instead of MLS approximations, and created a new and very accurate LBIE method. Although that paper solves almost all the problems appearing in the aforementioned works of [Sellountos and Polyzos (2003)], [Vavourakis and Polyzos (2007)] and [Vavourakis and Polyzos (2007)], it uses the same complicated integration technique of [Sellountos and Polyzos (2003)], which actually prevents the extension of the method to three dimensions.

The present paper demonstrates the use of the LBIE/RBF method for the solution of plane elastostatic problems. Its philosophy is different from that adopted in the previous work of [Sellountos, Sequeira, and Polyzos (2009)] and the extension of the present work to three dimensions seems to be straightforward. More precisely, non-uniformly distributed points taken from a Finite Element Method (FEM) mesh, cover the analyzed domain and form background cells with more than four points each. The FEM mesh determines the position of the points and it does not impose any connectivity requirement. The support domain of each point is divided into parts according to the background cells, and the RBF interpolation scheme of [Sellountos and Sequeira (2008a)], [Sellountos and Sequeira (2008b)] is exploited for the meshless representation of displacements in each cell. Tractions in the interior domain are avoided with the aid of the companion solution. At the intersections between the local domains and the global boundary, tractions are treated as independent variables with conventional boundary elements. The paper is organized as follows: in the next section the adopted LBIE formulation is illustrated. In Section 3 the numerical implementation of the method is addressed and criteria for the size of the support domains are provided. Finally, in Section 4 three benchmark problems are provided in order to demonstrate the accuracy of the proposed method.

2 LBIE formulation for elastostatics

Consider a two-dimensional linear and isotropic elastic domain V surrounded by a surface S. According to the classical theory of elasticity, the displacement vector $\mathbf{u}$ defined at any point $\mathbf{x}$ of the body satisfies the Navier-Cauchy partial differential equation

$$\mu\nabla^2\mathbf{u}(\mathbf{x}) + (\lambda+\mu)\nabla\nabla\cdot\mathbf{u}(\mathbf{x}) + \mathbf{b}(\mathbf{x}) = \mathbf{0} \tag{1}$$

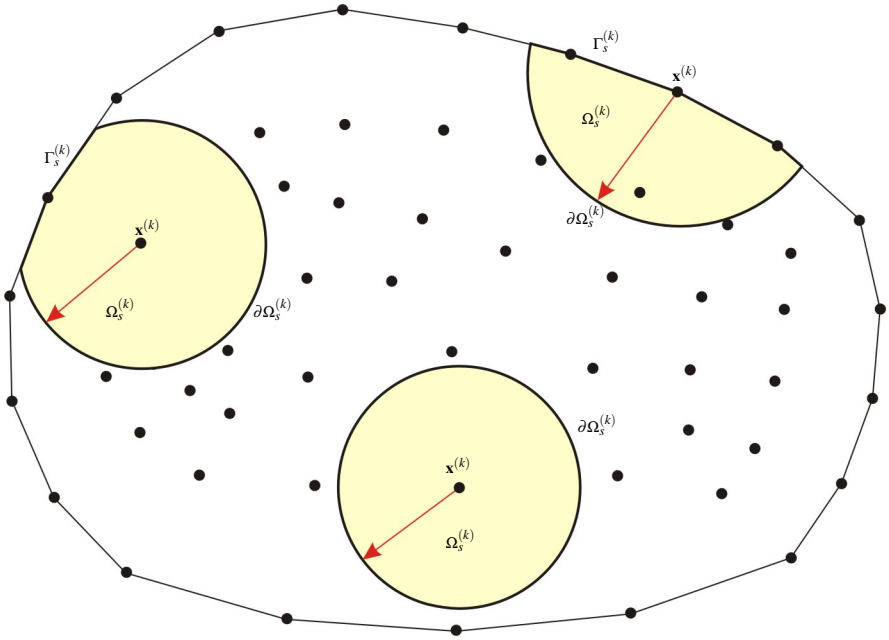

Figure 1: Local domains and boundaries used for the LBIE representation of discpacements at point $\mathbf{x}^k$

where λ and μ represent the Lamé constants, $\mathbf{b}$ indicates body forces and ∇ is the gradient operator.

The boundary conditions are assumed to be

$$\begin{aligned} \mathbf{u}(\mathbf{x}) &= \bar{\mathbf{u}}(\mathbf{x}) \ \text{ for } x \in S_u \\ \mathbf{t}(\mathbf{x}) &= \bar{\mathbf{t}}(\mathbf{x}) \ \text{ for } x \in S_t \end{aligned} \tag{2}$$

where $\mathbf{t}$ denotes the traction vector, $\bar{\mathbf{u}}$, $\bar{\mathbf{t}}$ represent prescribed vectors and $S_u \cup S_t \equiv S$. Any point $\mathbf{x}$ of the analyzed domain is considered to be the center of a local circular domain Ω_s (with boundary $\partial\Omega_s$) called support domain of $\mathbf{x}$ as illustrated in Fig. 1.

Considering zero body forces, employing the static fundamental solution of Eq. 1 and exploiting Betti's reciprocal identity, the following LBIE for the support do-

main of any interior or boundary point $\mathbf{x}$ is obtained [Sellountos and Polyzos (2003)]

$$\mathbf{u}(\mathbf{x}) + \int_{\partial\Omega_s} \mathbf{t}^*(\mathbf{x},\mathbf{y}) \cdot \mathbf{u}(\mathbf{y})\, dS_y = \int_{\partial\Omega_s} \mathbf{u}^*(\mathbf{x},\mathbf{y}) \cdot \mathbf{t}(\mathbf{y})\, dS_y \tag{3}$$

when the support domain is interior to V and

$$\alpha\mathbf{u}(\mathbf{x}) + \int_{\partial\Omega_s \cup \Gamma_s} \mathbf{t}^*(\mathbf{x},\mathbf{y}) \cdot \mathbf{u}(\mathbf{y})\, dS_y = \int_{\partial\Omega_s \cup \Gamma_s} \mathbf{u}^*(\mathbf{x},\mathbf{y}) \cdot \mathbf{t}(\mathbf{y})\, dS_y \tag{4}$$

when the support domain intersects the global boundary at $\Gamma_s \equiv \partial\Omega_s \cap S$. The coefficient α is equal to 1 for internal points and $1/2$ for points lying on the global boundary S, $\mathbf{u}^*$, $\mathbf{t}^*$ represent the fundamental displacement and traction tensors, respectively, given by [Polyzos, Tsinopoulos, and Beskos (1998)]

$$\mathbf{u}^* = \frac{1}{8\pi\mu(1-\nu)} \left[(4\nu-3)\ln r\mathbf{I} + \hat{\mathbf{r}} \otimes \hat{\mathbf{r}}\right] \tag{5}$$

$$\mathbf{t}^* = \frac{1}{2\pi}\left[\frac{1-2\nu}{2(1-\nu)}\frac{1}{r}(\hat{\mathbf{r}}\otimes\hat{\mathbf{n}} - \hat{\mathbf{n}}\otimes\hat{\mathbf{r}}) - \frac{1-2\nu}{2(1-\nu)}\frac{1}{r}(\hat{\mathbf{n}}\cdot\hat{\mathbf{r}})\mathbf{I} - \frac{1}{1-\nu}\frac{1}{r}(\hat{\mathbf{n}}\cdot\hat{\mathbf{r}})\hat{\mathbf{r}}\otimes\hat{\mathbf{r}}\right] \tag{6}$$

where $r = |\mathbf{y}-\mathbf{x}|$, $\otimes$ indicates dyadic product defined as $\mathbf{a}\otimes\mathbf{b} = a_i b_j \hat{\mathbf{x}}_i \otimes \hat{\mathbf{x}}_j$, with $i, j = 1, 2$ and $\hat{\mathbf{x}}_1, \hat{\mathbf{x}}_2$ being unit vectors of a Cartesian co- ordinate system and $\mathbf{I}$ is the unit tensor.

In order to eliminate traction vectors appearing in integrals defined on $\partial\Omega_s$, the use of the companion solution $\mathbf{u}^c$ is made [Atluri, Sladek, Sladek, and Zhu (2000)]. Thus the LBIEs Eq. 3 and Eq. 4 obtain the form, respectively

$$\mathbf{u}(\mathbf{x}) + \int_{\partial\Omega_s} [\mathbf{t}^*(\mathbf{x},\mathbf{y}) - \mathbf{t}^c(\mathbf{x},\mathbf{y})] \cdot \mathbf{u}(\mathbf{y})\, dS_y = \mathbf{0} \tag{7}$$

and

$$\alpha\mathbf{u}(\mathbf{x}) + \int_{\partial\Omega_s \cup \Gamma_s} [\mathbf{t}^*(\mathbf{x},\mathbf{y}) - \mathbf{t}^c(\mathbf{x},\mathbf{y})] \cdot \mathbf{u}(\mathbf{y})\, dS_y = \int_{\Gamma_s} [\mathbf{u}^*(\mathbf{x},\mathbf{y}) - \mathbf{u}^c(\mathbf{x},\mathbf{y})] \cdot \mathbf{t}(\mathbf{y})\, dS_y \tag{8}$$

where

$$\mathbf{u}^c = \frac{1}{8\pi\mu(1-\nu)}\frac{r^2}{r_0^2}\hat{\mathbf{r}}\otimes\hat{\mathbf{r}} + \frac{1}{8\pi\mu(1-\nu)}\left[\frac{5-4\nu}{2(3-4\nu)}\left(1-\frac{r^2}{r_0^2}\right) - (3-4\nu)\ln r_0\right]\mathbf{I} \tag{9}$$

$$\mathbf{t}^c = \frac{1}{4\pi(1-\nu)(3-4\nu)r_0^2}\left[3\hat{\mathbf{r}}\otimes\hat{\mathbf{n}} - \hat{\mathbf{n}}\otimes\hat{\mathbf{r}} - (\hat{\mathbf{n}}\cdot\hat{\mathbf{r}})\mathbf{I}\right] \tag{10}$$

with r_0 being the radius of the support domain Ω_s.

Replacing $\mathbf{u}^*(\mathbf{x},\mathbf{y}) - \mathbf{u}^c(\mathbf{x},\mathbf{y})$, $\mathbf{t}^*(\mathbf{x},\mathbf{y}) - \mathbf{t}^c(\mathbf{x},\mathbf{y})$ by $\mathbf{U}^*(\mathbf{x},\mathbf{y})$, $\mathbf{T}^*(\mathbf{x},\mathbf{y})$, respectively, Eqs Eq. 7 and Eq. 8 are written as

$$\mathbf{u}(\mathbf{x}) + \int_{\partial\Omega_s} \mathbf{T}^*(\mathbf{x},\mathbf{y})\cdot\mathbf{u}(\mathbf{y})\, dS_y = \mathbf{0} \tag{11}$$

and

$$\alpha\mathbf{u}(\mathbf{x}) + \int_{\partial\Omega_s\cup\Gamma_s} \mathbf{T}^*(\mathbf{x},\mathbf{y})\cdot\mathbf{u}(\mathbf{y})\, dS_y = \int_{\Gamma_s} \mathbf{U}^*(\mathbf{x},\mathbf{y})\cdot\mathbf{t}(\mathbf{y})\, dS_y \tag{12}$$

The integral Eq. 11 and Eq. 12 represent the LBIE of any interior and boundary point of the analyzed domain and in conjunction with cell RBFs explained below, they will be used in the proposed LBIE numerical scheme.

3 Interpolation and numerical implementation

In this section the numerical implementation of the proposed LBIE methodology is illustrated. The formulation is explained for both cases where the support domain intersects or not the global boundary.

Consider the elastic domain V of Fig. 1 covered by arbitrarily distributed points created by a FEM mesh. For the sake of simplicity, four point FEM elements are used. Each element corresponds to an RBF cell [Sellountos and Sequeira (2008b)] with four points. An internal point $\mathbf{x}^k$ with support domain $\partial\Omega_s^{(k)}$ (Fig. 2) is considered. The nearby points $\mathbf{x}^1,\mathbf{x}^2,...,\mathbf{x}^8$, form four cells that separate the local boundary $\partial\Omega_s^{(k)}$ into the arcs $\partial\Omega_{s^{(1)}}^{(k)}, \partial\Omega_{s^{(2)}}^{(k)}, ..., \partial\Omega_{s^{(4)}}^{(k)}$. Then, Eq. 11 valid for the support domain of point $\mathbf{x}^k$ takes the form

$$\mathbf{u}\left(\mathbf{x}^{(k)}\right) + \int_{\partial\Omega_{s^{(1)}}^{(k)}} \mathbf{T}^*(\mathbf{x},\mathbf{y})\cdot\mathbf{u}(\mathbf{y})\, dS_y + ... + \int_{\partial\Omega_{s^{(4)}}^{(k)}} \mathbf{T}^*(\mathbf{x},\mathbf{y})\cdot\mathbf{u}(\mathbf{y})\, dS_y = \mathbf{0} \tag{13}$$

At any cell, the displacement field is approximated via a local RBF interpolation scheme illustrated in [Sellountos and Sequeira (2008b)], i.e.

$$\mathbf{u}(\mathbf{y}) = \mathbf{R}\left(\mathbf{y},\mathbf{x}^{(j)}\right)\cdot\mathbf{u}\left(\mathbf{x}^{(j)}\right) \tag{14}$$

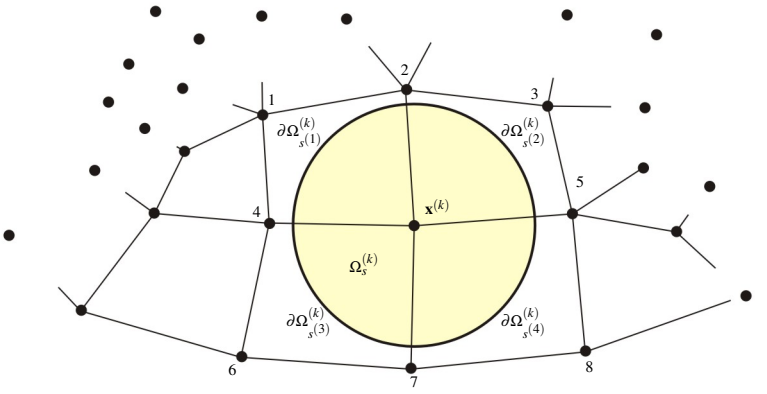

Figure 2: Internal point and its support domain being internal to the domain of interest divided by the cells

By inserting Eq. 14 into Eq. 13, the following discretized equation is obtained

$$\mathbf{u}\left(\mathbf{x}^{(k)}\right)+\int_{\partial\Omega_{s(1)}^{(k)}}\mathbf{T}^{*}\left(\mathbf{x},\mathbf{y}\right)\cdot\mathbf{R}^{(1)}\,dS_{y}\cdot\begin{bmatrix}\mathbf{u}^{(1)}\\ \mathbf{u}^{(2)}\\ \mathbf{u}^{(4)}\\ \mathbf{u}^{(k)}\end{bmatrix}+\ldots+$$

$$\int_{\partial\Omega_{s(4)}^{(k)}}\mathbf{T}^{*}\left(\mathbf{x},\mathbf{y}\right)\cdot\mathbf{R}^{(4)}\,dS_{y}\cdot\begin{bmatrix}\mathbf{u}^{(k)}\\ \mathbf{u}^{(5)}\\ \mathbf{u}^{(7)}\\ \mathbf{u}^{(8)}\end{bmatrix}=\mathbf{0} \tag{15}$$

As it has been mentioned, more than four points per cell can be used for the RBF representation of the displacement field at any cell. This depends on the degree of the RBF interpolation scheme imposed in the analyzed fields, and it is accomplished with the aid of higher order FEM geometric elements. Each point has its own support domain with a radius belonging in to the range $(r_{min}^{(k)}, r_{max}^{(k)})$, with $r_{min}^{(k)}$ being the minimum distance between $\mathbf{x}^{(k)}$ and the opposite sides of the cell, and $r_{max}^{(k)}$ is the maximum distance between $\mathbf{x}^{(k)}$ and the cell's corner nodes. Both $r_{min}^{(k)}, r_{max}^{(k)}$ are illustrated in Fig. 3. In case where $\mathbf{x}^{(k)}$ is a boundary point and its support domain intersects the global boundary S, the geometric FEM cells separate

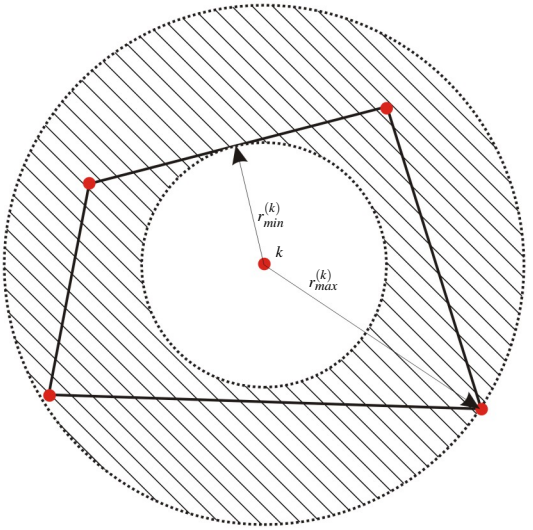

(a)

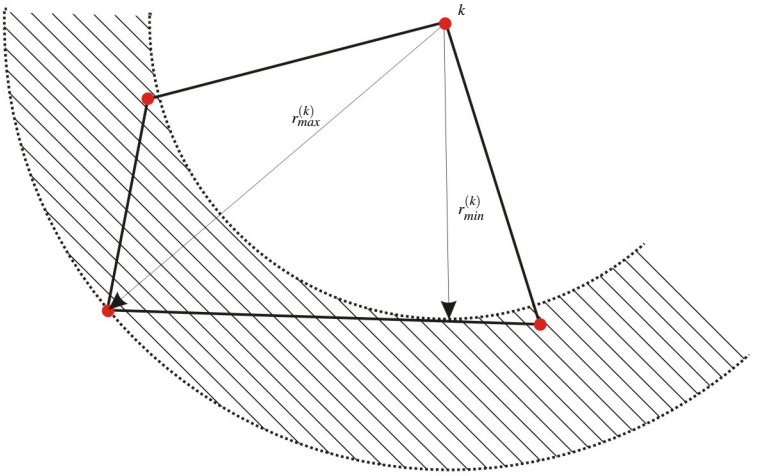

(b)

Figure 3: Definition of support domain range (shadow area) (a) for an internal cell point and (b) for a corner cell point

the circular boundary $\partial\Omega_s^{(k)}$ and the global boundary $\Gamma_s^{(k)}$ into parts as shown in Fig. 4. The displacement field at any cell is interpolated with the aid of the RBF interpolation scheme and the tractions on the boundary are treated as independent variables with the usage of linear or quadratic boundary elements.

Thus the LBIE Eq. 12 takes the form

$$\begin{aligned}
\frac{1}{2}\mathbf{u}\left(\mathbf{x}^{(k)}\right) + \int_{\Gamma_{s^{(1)}}^{(k)} \cup \partial\Omega_{s^{(1)}}^{(k)}} \mathbf{T}^*\left(\mathbf{x},\mathbf{y}\right)\cdot\mathbf{R}^{(1)}\, dS_y \cdot \begin{bmatrix} \mathbf{u}^{(1)} \\ \mathbf{u}^{(2)} \\ \mathbf{u}^{(5)} \\ \mathbf{u}^{(6)} \end{bmatrix} + \\
\int_{\Gamma_{s^{(2)}}^{(k)} \cup \partial\Omega_{s^{(2)}}^{(k)}} \mathbf{T}^*\left(\mathbf{x},\mathbf{y}\right)\cdot\mathbf{R}^{(2)}\, dS_y \cdot \begin{bmatrix} \mathbf{u}^{(2)} \\ \mathbf{u}^{(k)} \\ \mathbf{u}^{(6)} \\ \mathbf{u}^{(7)} \end{bmatrix} + \\
\int_{\partial\Omega_{s^{(3)}}^{(k)}} \mathbf{T}^*\left(\mathbf{x},\mathbf{y}\right)\cdot\mathbf{R}^{(3)}\, dS_y \cdot \begin{bmatrix} \mathbf{u}^{(6)} \\ \mathbf{u}^{(7)} \\ \mathbf{u}^{(10)} \\ \mathbf{u}^{(11)} \end{bmatrix} + \ldots + \\
\int_{\Gamma_{s^{(4)}}^{(k)} \cup \partial\Omega_{s^{(6)}}^{(k)}} \mathbf{T}^*\left(\mathbf{x},\mathbf{y}\right)\cdot\mathbf{R}^{(6)}\, dS_y \cdot \begin{bmatrix} \mathbf{u}^{(3)} \\ \mathbf{u}^{(4)} \\ \mathbf{u}^{(8)} \\ \mathbf{u}^{(9)} \end{bmatrix} = \\
\int_{\Gamma_{s^{(1)}}^{(k)}} \mathbf{U}^*\left(\mathbf{x},\mathbf{y}\right)\cdot\mathbf{N}^{(1)}\, dS_y \cdot \begin{bmatrix} \mathbf{t}^{(1)} \\ \mathbf{t}^{(2)} \end{bmatrix} + \ldots + \int_{\Gamma_{s^{(4)}}^{(k)}} \mathbf{U}^*\left(\mathbf{x},\mathbf{y}\right)\cdot\mathbf{N}^{(4)}\, dS_y \cdot \begin{bmatrix} \mathbf{t}^{(3)} \\ \mathbf{t}^{(4)} \end{bmatrix}
\end{aligned} \tag{16}$$

where $\mathbf{N}$ is the matrix containing the interpolation functions of the boundary elements defined by the nodes $\mathbf{x}^{(1)}, \mathbf{x}^{(2)}, \mathbf{x}^{(k)}, \mathbf{x}^{(3)}, \mathbf{x}^{(4)}$. Observing Eq. 16, it is easy to see that the boundary conditions of the problem are directly imposed via the values of $\mathbf{u}$ and $\mathbf{t}$ at the nodes $1, 2, k, 3$ and 4. Deriving the LBIEs for all points according to Eq. 14 and Eq. 16, imposing the boundary conditions Eq. 2 and rearranging the system coefficients, the system of algebraic equations

$$\tilde{\mathbf{A}} \cdot \mathbf{X} = \mathbf{b} \tag{17}$$

is obtained, where the vector $\mathbf{X}$ is composed of all unknown displacements and boundary tractions. The matrix $\tilde{\mathbf{A}}$ has sparse or band form. Finally, by solving the above system of equations with an LU decomposition solver, the displacements and

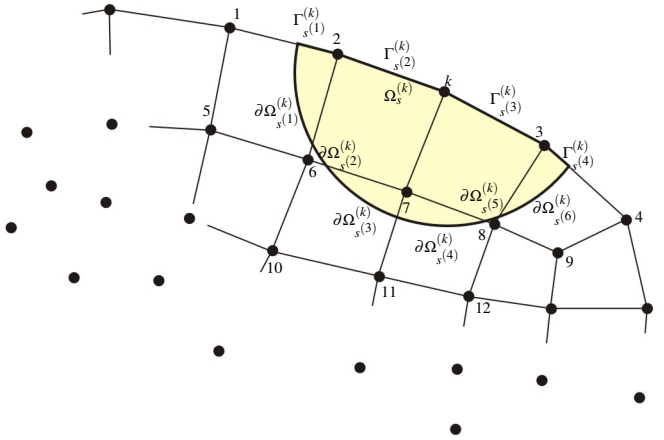

Figure 4: Boundary point and its support domain intersected by the global boundary and divided by the cells

boundary tractions are provided. The stresses can be evaluated either by differentiating displacements as in FEM, or by using the hypersingular LBIE.

4 Numerical examples

The achieved accuracy of the proposed LBIE method is demonstrated in the present section by solving three representative elastic problems.

4.1 Cantilever beam

The first problem deals with a clamped cantilever beam subjected to a shear load at its right free-end (Fig. 5) under conditions of plane strain. The analytical solution of the problem can be found in the book of [Timoshenko and Goodier (1970)]. Thickness and length are H=1m and L=10m, respectively, Young modulus $E = 10^5 Pa$, Poisson ratio $\nu = 0.1$ and shear load $P = 1Pa$. Two meshes with nine-noded elements have been used for the definition of the cells, as it is depicted in Fig. 6. Fig. 7 depicts axial displacements across the axis of symmetry of the beam, while Fig. 8 portrays axial tractions on the clambed side. Both figures show very good agreement with analytical solutions. Finally, in Fig. 9 and Fig. 10 the axial stresses on two cross-sections of the beam obtained by differentiating the RBF representation of displacements and exploiting Hooke's law are presented. The

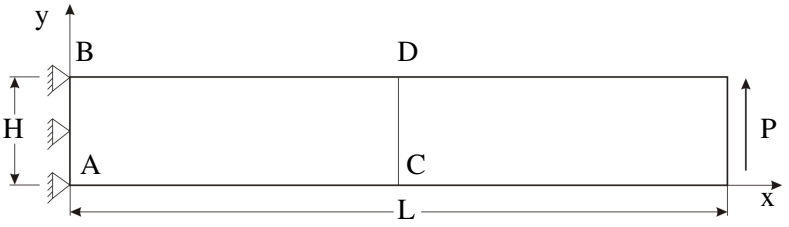

Figure 5: Cantilever beam subjected to a flexular load P.

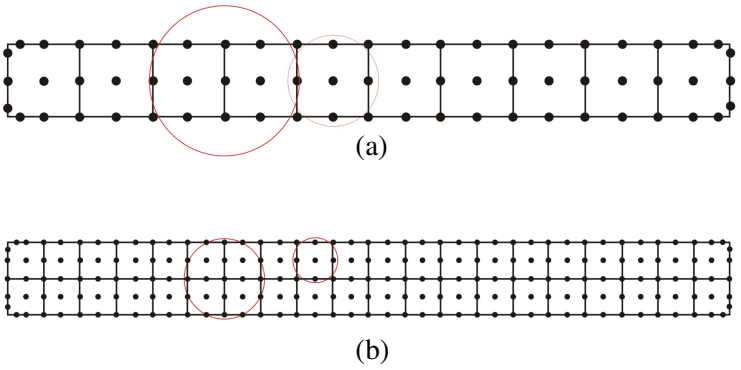

Figure 6: Meshes used for the cantilever beam problem, (a) a coarse mesh with 10 cells and 67 nodal points and (b) a fine mesh with 40 cells and 209 nodal points

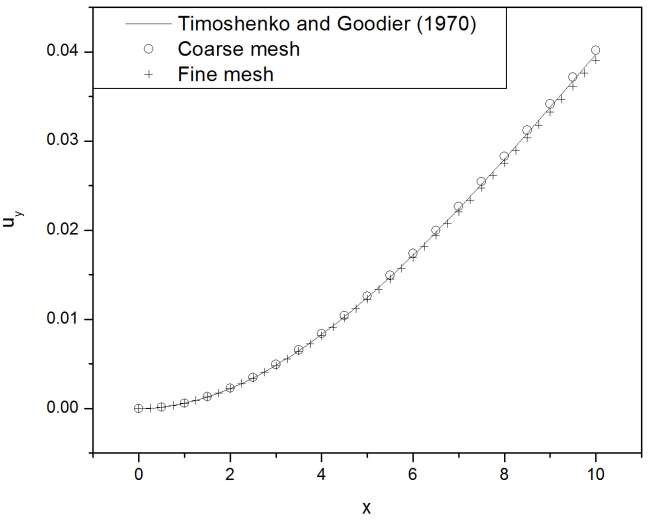

Figure 7: Vertical displacements along the axis of symmetry $y = 0.5$ m of the cantilever beam.

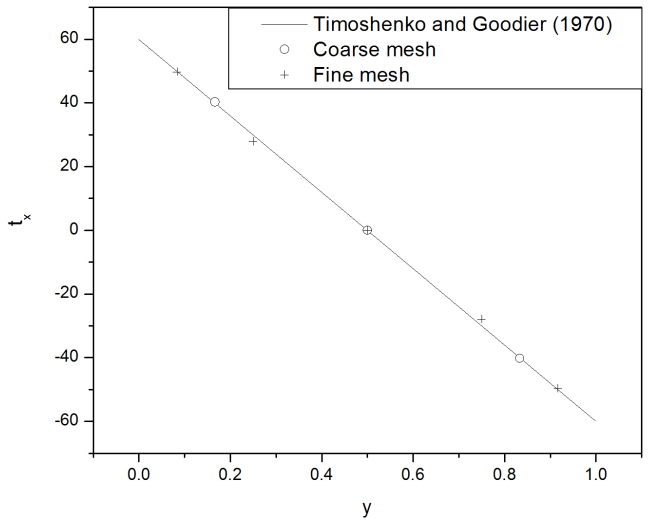

Figure 8: Axial tractions along the line AB of the cantilever beam.

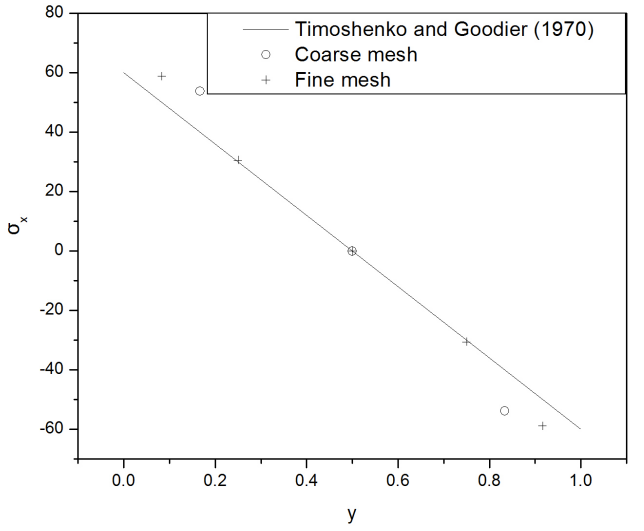

Figure 9: Axial stresses along the line AB of the cantilever beam.

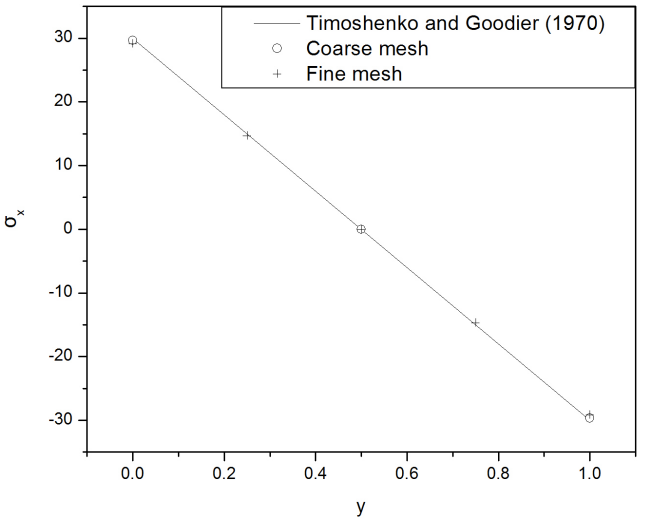

Figure 10: Axial stresses along the line CD of the cantilever beam.

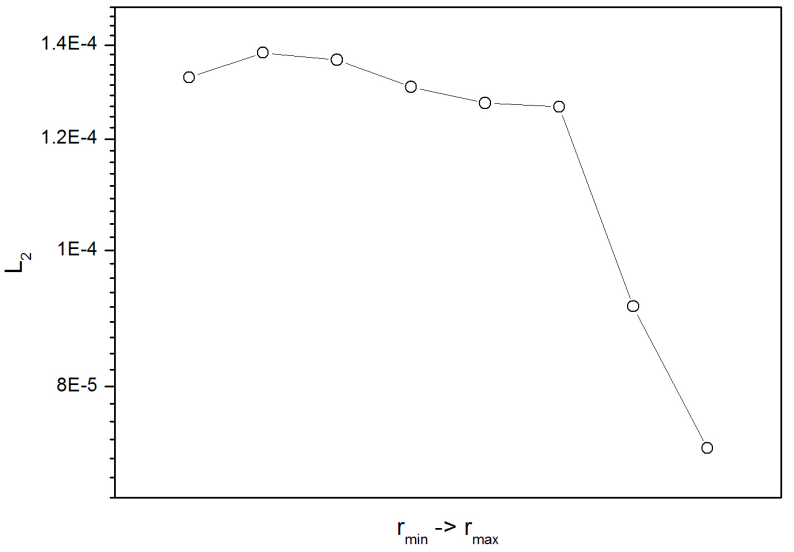

Figure 11: L2 Convergence norm of the displacements of the cantilever beam for support domains in the area r_{min} - r_{max}

agreement of the present results with those of the analytical solutions is again very good.

In order to demonstrate the influence of the support domain's size to obtained results, a parametric study for different support domain radii (being between r_{min} and r_{max}) is performed and the *L2*-error norm defined as

$$L_2 = \frac{1}{N}\sqrt{\frac{\Sigma_{i=1}^{N}||\hat{\mathbf{u}}^i - \mathbf{u}^i||}{\Sigma_{i=1}^{N}||\hat{\mathbf{u}}^i||}} \tag{18}$$

is depicted in Fig. 11. In Eq. 18 $N, \hat{\mathbf{u}}^i, \mathbf{u}^i$ represent the number of nodal points, the analytical and the achieved numerical solution. As it is apparent from Fig. 11, the best accuracy is obtained for support domains having value close to r_{max}. However, as the support domain is getting bigger, the accuracy is getting higher, for domains with $r < r_{min}$ or $r > r_{max}$ the solution appear to be unstable. This is due to the fact that for support domains with radius r out of the limits r_{min}, r_{max} the coupling of

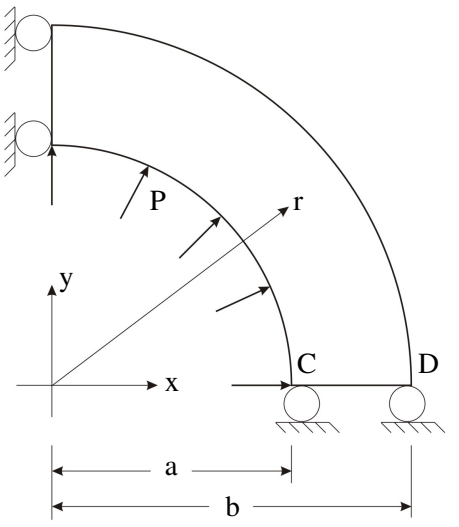

Figure 12: Cylinder subjected to internal pressure

LBIEs becomes many times "non- uniform" thus affecting negatively the formation of the final system of algebraic equations.

4.2 Cylinder subjected to internal pressure

The second problem deals with a circular cylinder with inner and outer radius $a = 1m$ and $b = 2m$, respectively, subjected to a uniform internal pressure $P = 1Pa$. The material properties are taken $E = 10^5 Pa$ for Young modulus and $\nu = 0.1$ for Poisson ratio. Because of the symmetry only a quarter part of the cylinder is analyzed (Fig. 12). As in the previous example, two different distributions of points have been used (Fig. 13). The analytical radial displacements and stresses of this problem, expressed in polar coordinates are given in [Timoshenko and Goodier (1970)]. The radial displacement and the traction field along the line CD of the cylinder (Fig. 12) are numerically evaluated and compared to analytical solutions as shown in Fig. 14 and Fig. 15, respectively. As it is evident, the agreement between numerical and analytical results is very good. Radial and hoop stresses along the line CD of the cylinder are calculated by differentiating the RBF representation of displacements and exploiting Hooke's law. Analytical and numerical results are presented in Fig. 16 and Fig. 17 and appear to be in very good agreement bewteen them.

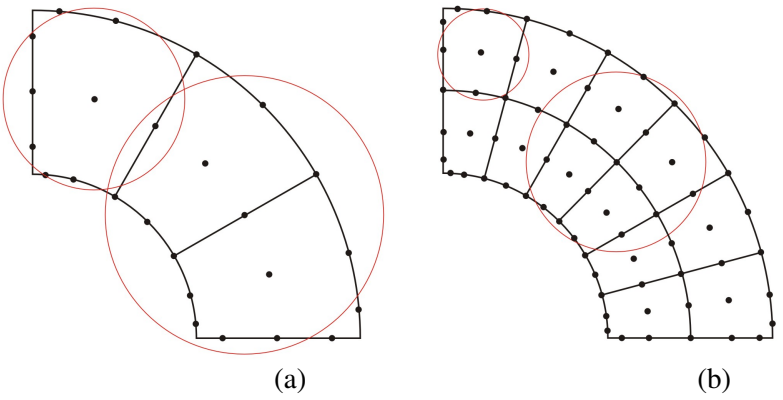

Figure 13: Meshes used for the solution of the cylinder under internal pressure, (a) a coarse mesh with 3 cells and 25 nodes and (b) a fine mesh with 12 cells and 69 nodes

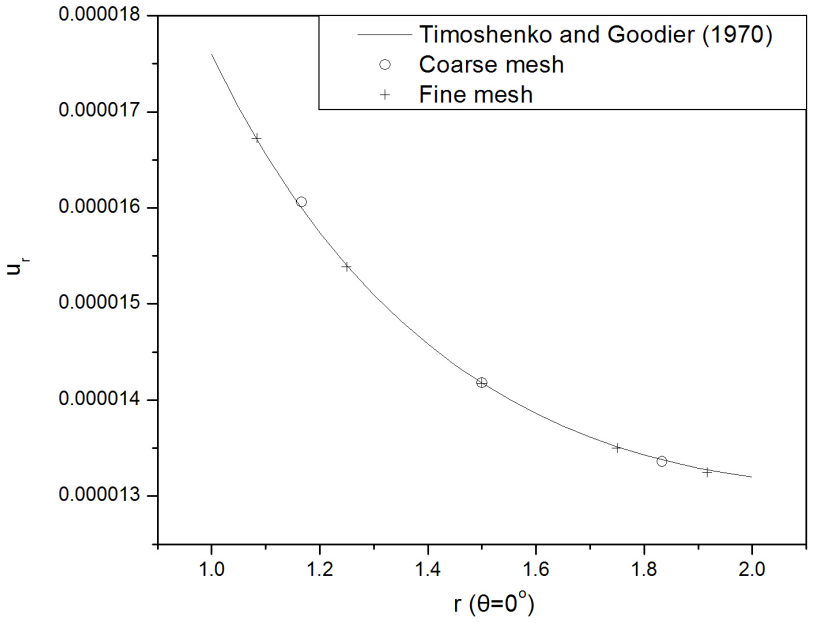

Figure 14: Radial displacements along the line CD of the cylinder.

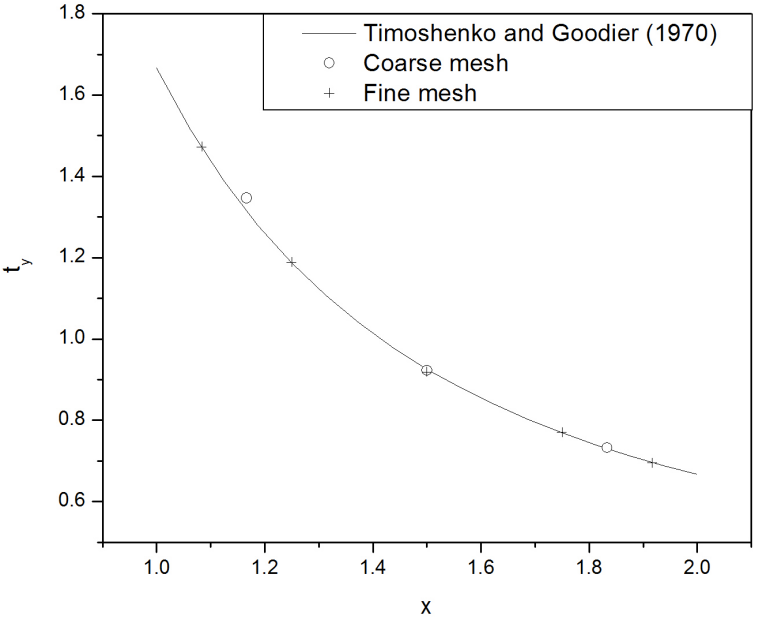

Figure 15: Tractions t_y along the line CD of the cylinder.

4.3 Kirsch plate

The third problem deals with a $60m$ x $60m$ plate with a circular hole of radius $a = 1m$ at its center, subjected to a uniform tensile load $p = 1Pa$ (Fig. 18). The material properties are assumed to be $E = 10^5 Pa$ and $\nu = 1$. Due to the symmetry, only the upper right quadrant of the plate is analyzed, while two different meshes depicted in Fig. 19 are used. All obtained results are compared with the analytical solutions provided in [Timoshenko and Goodier (1970)]. Fig. 20, Fig. 21, Fig. 22 and Fig. 23 portray displacements and tractions along the sides AB and CD. Finally, stresses along the side AB and CD are evaluated as in the previous two examples and they are depicted in Fig. 24, Fig. 25, Fig. 26 and Fig. 27. All the obtained numerical results show a good agreement with the analytical solutions.

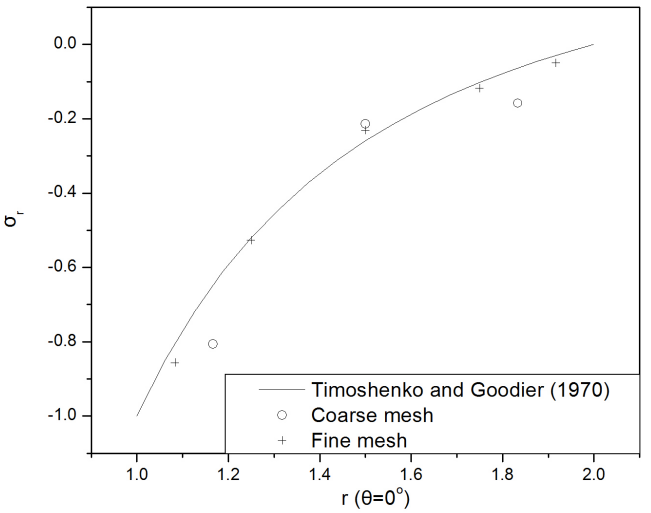

Figure 16: Radial stresses along the line CD of the cylinder.

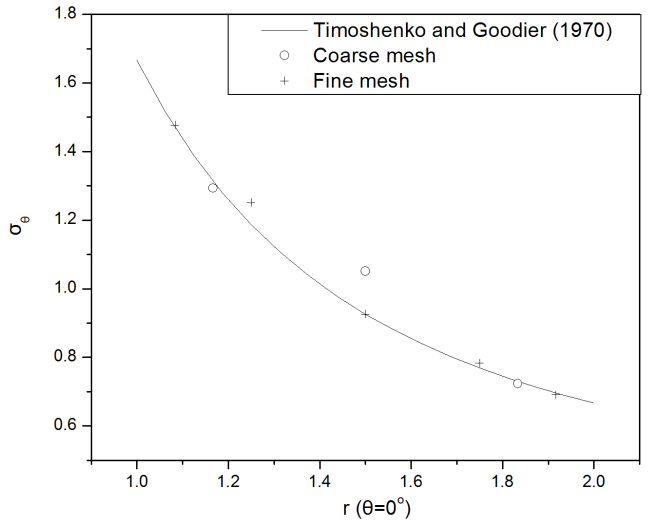

Figure 17: Hoop (b) stresses along the line CD of the cylinder.

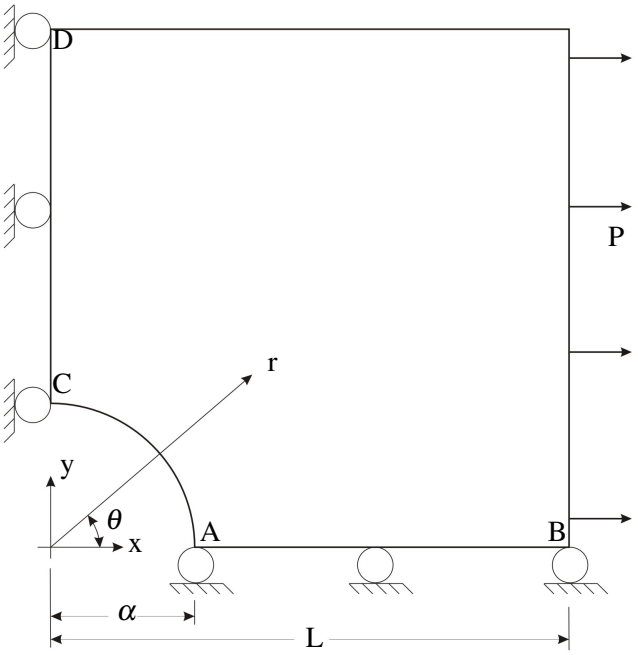

Figure 18: Perforated plate under uniform tension P

5 Conclusions

A local boundary integral equation (LBIE) method for solving two dimensional elastic problems has been proposed. Points taken from a Finite Element Method (FEM) mesh cover the analyzed domain and form background cells. The support domain of each point is divided into parts via the background cells, and the Radial Basis Functions (RBF) interpolation scheme of [Sellountos and Sequeira (2008b)] is exploited for the representation of displacements in each cell. Each point has its own support domain with radius taking values in an interval, defined after parametric studies carried out in the context of the present work. In the interior domain, tractions are eliminated with the aid of the companion solution. At the global boundary, tractions are treated as independent variables via line quadratic elements, while the final system of algebraic equations is sparse or in banded form. The three numerical examples considered here have shown that the accuracy of the method is very good even for a coarse distribution of points. The most important feature of the proposed LBIE/RBF technique is that its extension to three dimensional problems

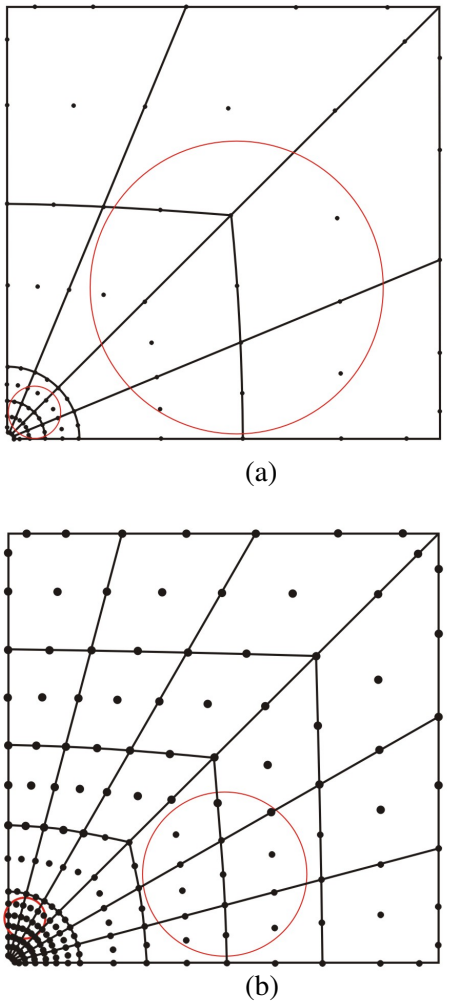

Figure 19: Meshes used for the solution of the kirsch plate, (a) a coarse mesh with 16 cells and 87 nodes, and (b) a fine mesh with 42 cells and 201 nodes

seems to be straightforward.

Acknowledgement: This work has been partially supported by the Center of

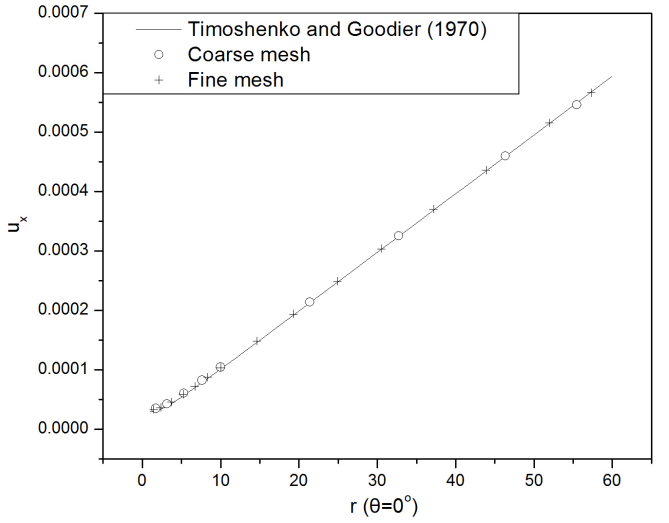

Figure 20: u_x displacements along the side AB of the perforated plate

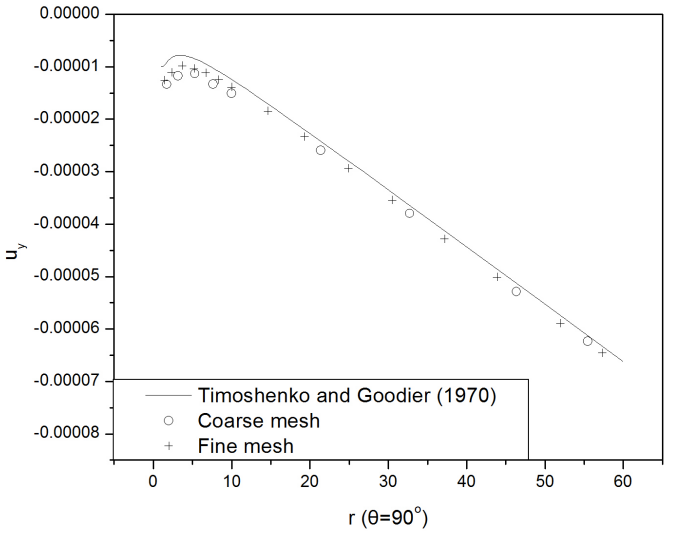

Figure 21: u_y displacements along the CD side of the perforated plate

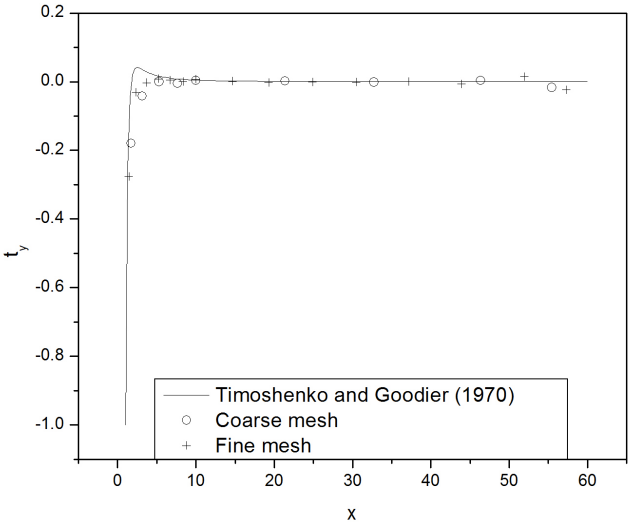

Figure 22: t_y tractions along the side AB of the perforated plate

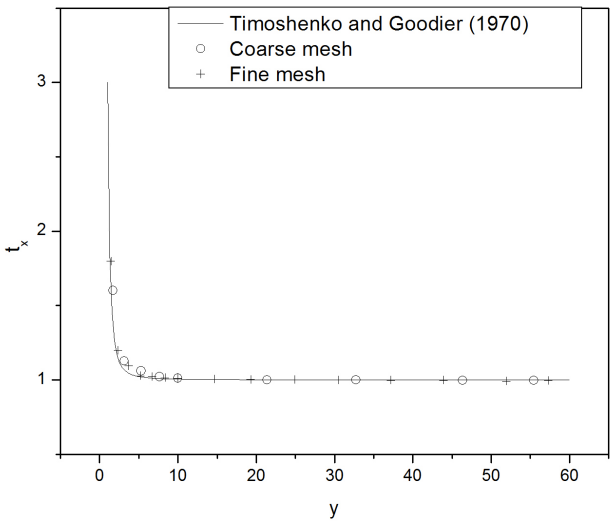

Figure 23: t_x tractions along the side CD of the perforated plate

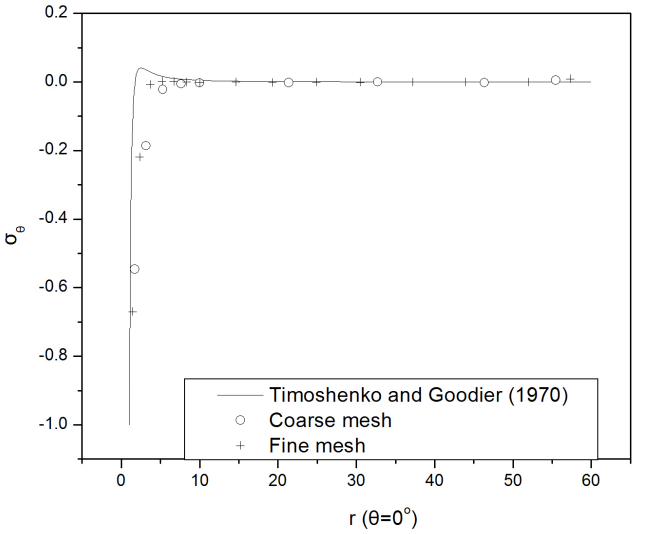

Figure 24: σ_θ stresses along the side AB ($y = 0, \theta = 0^o$, for the perforated plate)

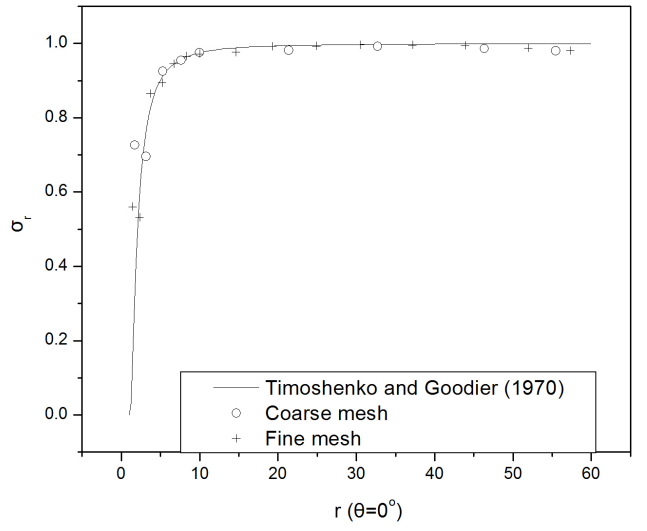

Figure 25: σ_r stresses along the side AB ($y = 0, \theta = 0^o$, for the perforated plate)

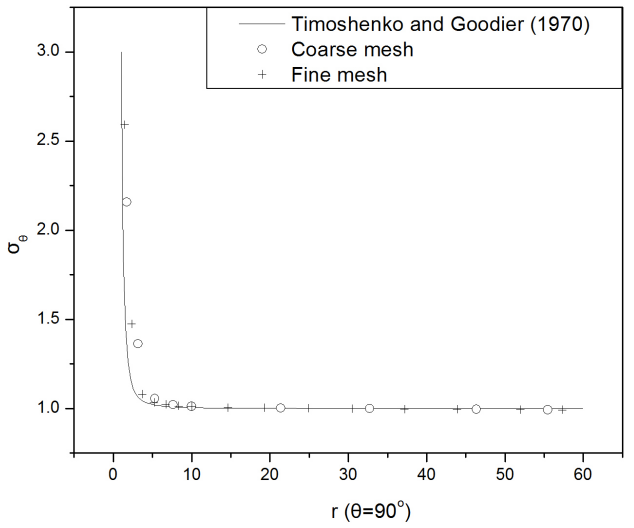

Figure 26: σ_θ stresses along the side CD ($x = 0, \theta = 90^o$, for the perforated plate)

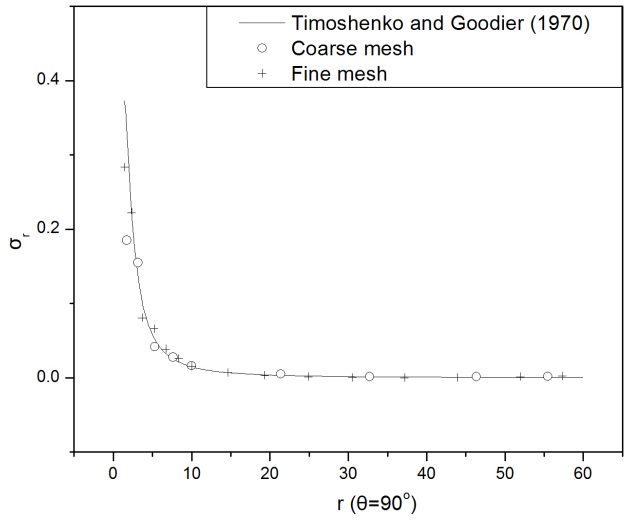

Figure 27: σ_r stresses along the side CD ($x = 0, \theta = 90^o$, for the perforated plate)

Mathematics and its Applications (CEMAT/IST) through FCT's Funding Program and by the grant Ciência 2008 of FCT (E.J.Sellountos)

References

Atluri, S. N. (2004): *The meshless method (MLPG) for domain & BIE discretizations*. Tech. Science Press.

Atluri, S. N.; Han, Z. D.; Shen, S. (2003): Meshless local Petrov-Galerkin (MLPG) approaches for solving the weakly-singular traction and displacement boundary integral equations. *CMES: Computer Modeling in Engineering & Sciences*, vol. 4, pp. 507–517.

Atluri, S. N.; Shen, S. (2002): *The Meshless Local Petrov-Galerkin (MLPG) Method*. Tech. Science Press.

Atluri, S. N.; Sladek, J.; Sladek, V.; Zhu, T. (2000): The local boundary integral equation (LBIE) and its meshless implementation for linear elasticity. *Comput. Mech.*, vol. 25, pp. 180–198.

Bodin, A.; Ma, J.; Xin, X. J.; Krishnaswami, P. (2006): A meshless integral method based on regularized boundary integral equation. *Computer Methods in Applied Mechanics and Engineering*, vol. 195, pp. 6258–6286.

Gosz, S.; Liu, W. (1996): Admissible approximations for essential boundary conditions in the reproducing kernel particle method. *Computational Mechanics*, vol. 19, pp. 120–135.

Han, Z. D.; Atluri, S. N. (2003): On simple formulations of weaklysingular traction & displacement BIE, and their solutions through Petrov Galerkin approaches. *CMES: Computer Modeling in Engineering & Sciences*, vol. 4, pp. 5–20.

Polyzos, D.; Tsinopoulos, S. V.; Beskos, D. E. (1998): Static and dynamic boundary element analysis in incompressible linear elasticity. *European. J. Mech. A/Solids*, vol. 17, pp. 515–536.

Sellountos, E. J.; Polyzos, D. (2003): A MLPG (LBIE) method for solving frequency domain elastic problems. *CMES: Computer Modelling in Engineering & Sciences*, vol. 4, pp. 619–636.

Sellountos, E. J.; Polyzos, D. (2005): A meshless local boundary integral equation method for solving transient elastodynamic problems. *Computational Mechanics*, vol. 35, pp. 265–276.

Sellountos, E. J.; Polyzos, D. (2005): A MLPG (LBIE) approach in combination with BEM. *Computer Methods in Applied Mechanics and Engineering*, vol. 194, pp. 859–875.

Sellountos, E. J.; Sequeira, A. (2008a): An advanced meshless LBIE/RBF method for solving two-dimensional incompressible fluid flows. *Computational Mechanics*, vol. 41, pp. 617–631.

Sellountos, E. J.; Sequeira, A. (2008b): A HybridMulti-Region BEM / LBIE-RBF Velocity-Vorticity Scheme for the Two-Dimensional Navier-Stokes Equations. *CMES: Computer Modelling in Engineering & Sciences*, vol. 23, pp. 127–147.

Sellountos, E. J.; Sequeira, A.; Polyzos, D. (2009): Elastic transient analysis with MLPG(LBIE) method and local RBFs. *CMES: Computer Modelling in Engineering & Sciences*, vol. 41, pp. 215–242.

Sellountos, E. J.; Vavourakis, V.; Polyzos, D. (2005): A new Singular / Hypersingular MLPG (LBIE) method for 2D elastostatics. *CMES: Computer Modelling in Engineering & Sciences*, vol. 7, pp. 35–48.

Sladek, J.; Sladek, V.; Atluri, S. (2002): Application of the local boundary integral equation method to boundary value problems. *International Journal of Applied Mechanics*, vol. 38, pp. 1025–1043.

Sladek, J.; Sladek, V.; Atluri, S. N.; Keer, R. V. V. (2000): Numerical integration of singularities of local boundary integral equations. *Comput. Mech.*, vol. 25, pp. 394–403.

Sladek, J.; Sladek, V.; Keer, R. V. V. (2003): Meshless local boundary integral equation method for 2D elastodynamic problems. *Int. J. Numer. Meth. Engng*, vol. 57, pp. 235–249.

Sladek, J.; Sladek, V.; Solek, P.; Tan, C. L.; Zhang, C. (2009): Two and three dimensional thermoelastic analysis by the MLPG method. *CMES: Computer Modelling in Engineering & Sciences*, vol. 47, pp. 61–96.

Timoshenko, S. P.; Goodier, J. N. (1970): *Theory of Elasticity*. McGraw-Hill 3rd Edition, New York.

Vavourakis, V. (2008): A local hypersingular integral equation method using triangular background mesh. *CMES: Computer Modelling in Engineering & Sciences*, vol. 36, pp. 119–146.

Vavourakis, V. (2009): A meshless local boundary integral equation method for two-dimensional steady elliptic problems. *Computational Mechanics*, vol. 44, pp. 777–790.

Vavourakis, V.; Polyzos, D. (2007): A new MLPG(LBIE) method for solving 2D elastostatic problems. *CMC: Computers Materials and Continua*, vol. 5, pp. 185–196.

Vavourakis, V.; Polyzos, D. (2008): A MLPG(LBIE) numerical method for solving 2D incompressible and nearly incompressible elastostatic problems. *Communications in Numerical Methods in Engineering*, vol. 24, pp. 281–296.

Vavourakis, V.; Protopappas, V. I. C.; Fotiadis, D.; Polyzos, D. (2009): Numerical determination of modal dispersion and AE signals characterization in waveguides through LBIE/BEM and time-frequency analysis. *Computational Mechanics*, vol. 43, pp. 431–441.

Vavourakis, V.; Sellountos, E. J.; Polyzos, D. (2006): A comparison study on different MLPG(LBIE) formulations. *CMES: Computer Modelling in Engineering & Sciences*, vol. 13, pp. 171–184.

Zhu, T.; Zhang, J.; Wang, D. (2007): A meshless Local Petrov-Galerkin (MLPG) approach based on the regular local boundary integral equation for linear elasticity. *Int. J. Comput. Methods in Enng Sci. and Mechanics*, vol. 8, pp. 373–382.

Zhu, T.; Zhang, J. D.; Atluri, S. N. (1998): A local boundary integral equation (LBIE) method in computational mechanics and a meshless discretization approach. *Comput. Mech.*, vol. 21, pp. 223–235.